Journal of Sound and Vibration (1995) **181**(4), 687–707

THE CELL TO CELL MAPPING TECHNIQUE AND CHAPMAN–KOLMOGOROV REPRESENTATION OF SYSTEM DYNAMICS

M. Belhadj and T. Aldemir

Nuclear Engineering Program, 1079 *Robinson Laboratory*, *The Ohio State University*, *Columbus*, *Ohio* 43210-1107, *U.S.A.*

(*Received* 13 *August* 1992, *and in final form* 24 *January* 1994)

The cell to cell mapping technique (CCMT) is a numerical technique for the global analysis of non-linear dynamic systems. The CCMT is particularly useful if the system has a strange attractor. Using a Chapman–Kolmogorov representation of system dynamics, two new CCMT algorithms are presented which substantially reduce the computational time and computer storage requirements compared to the conventional implementation of CCMT in the determination of the attractors of the system and their domains of attraction. The new algorithms are also advantageous when it is difficult to identify a unique probability density function (pdf) to represent the uncertainty in the system parameters and several pdfs need to be considered to assess the impact of the choice of the pdf on the predicted asymptotic system behavior. These features of the new algorithms are illustrated using a second order Duffing oscillator under harmonic forcing.

1. INTRODUCTION

In recent years there has been ample experimental [1–16] and theoretical [3, 5, 7, 8, 14, 17–19] evidence that the qualitative and quantitative features of the time evolution of non-linear dynamic systems can change drastically with a small change in system parameters and/or initial conditions. In that respect, global analysis of non-linear systems through investigating the variations in the structure of their attractors and their domains of attraction (DOAs) is important in order to understand the fault tolerance as well as the safety margins of the system under consideration. An attractor is a compact region in the system state space that is asymptotically reached in time by the dynamical system [8]. An attractor that is not a finite set of points, a limit cycle, a piecewise smooth surface, or bounded by a piecewise smooth closed surface volume is called a strange attractor [8]. Strange attractors are important for systems with chaotic behavior. The DOA of an attractor is a range of values of initial conditions (or a set of points in the system state space) that eventually lead to the attractor [8].

Global analysis by the direct numerical integration of the system equations can be a very time consuming, if not an infeasible task, particularly if the asymptotic system behavior is chaotic [12, 18, 20]. Also, uncertainties on the system parameters (e.g., due to possible experimental error or random fluctuations) may affect the attractor boundaries, "blurring" the DOA's [15]. While numerous fast techniques have been proposed to determine the stability of the equilibrium states and periodic solutions of non-linear systems as a function of the system parameters [8–10, 14, 17, 18, 21, 22], only two methods are found in the

0022–460X/95/140687 + 21 $08.00/0

literature that are suitable for global analysis in the sense described above when the system has higher than two degrees of freedom. These methods are: (1) global perturbation of invariant manifolds [19], which is mainly analytical and will be referred to as Wiggins method; and (2) the cell to cell mapping technique (CCMT) proposed by C. S. Hsu [23, 24], which represents the system dynamics by a Markov chain in discrete time and system state space.

Within the context of global analysis, an invariant manifold is a region in the state space of the dynamical system with the property that a trajectory starting from this region remains within the region throughout the course of its evolution. The Wiggins method is very powerful and straightforward if all the invariant manifolds consist of fixed points in the state space. However, the method requires the differentiability of the governing equations with respect to the system parameters (at least twice and six-fold in some cases) and also some prior knowledge of state space topology. When the invariant manifolds consist not only of fixed points but also contain periodic and chaotic trajectories, global analysis becomes a tedious, if not impossible, task. For example, the Wiggins method can prove that a system has a chaotic attractor, by using an analytical technique developed by Melkinov [25], but cannot determine the envelope of the chaotic attractor or its statistical properties, which can be important in the reliability and safety assessment of system operation.

Hsu's method (i.e., CCMT) is a numerical technique in which dynamic system evolution is modelled as a mapping or probability of trajectory transitions between specified computational cells (dynamic variable mangitude intervals) that partition the system state space. An overview of CCMT as described in references [23, 24] is given in section 2. One of the most attractive features of CCMT *vis-à-vis* the Wiggins method is that CCMT combines computational speed with a wide range of applicability. For example, Xu *et al*. [26] have shown that CCMT can determine the attractors in the four-dimensional state space of a coupled two-degree-of-freedom van der Pol system 200 times faster that direct numerical integration. Again, Hsu and Kim [27] have shown that the statistical properties of the strange attractor of a "stretch–contraction–reposition" map [28] can be determined by the CCMT eight times faster than the direct integration method for the same accuracy. Over 40 such studies have been reported in the literature by Hsu and his co-workers using various types of systems during the past ten years. Since CCMT has no differentiability requirements on the governing equations, it is perhaps the only computationally feasible technique that can be used for the global analysis of systems the configuration of which may change as a function of system parameters (e.g., a process control system with on/off controls), or systems the governing equations of which may be buried in a complex, hard-wired simulator which has the system parameters as inputs (as is often encountered in practice). Finally, its probabilistic modelling of system dynamics makes CCMT naturally suited for the global analysis of systems with stochastic parameters, as demonstrated by Hsu [23], Chiu and Hsu [29] and Sun and Hsu [30], and/or when there is uncertainty on the initial conditions.

Even with CCMT, the computational requirements for global analysis can be still prohibitive for practical systems. The purpose of this paper is to present two algorithms based on a Chapman–Kolmogorov representation of system dynamics (section 3.1) which reduce these computational requirements in the determination of: (a) the limiting probability distribution of the attractors when a unique probability distribtion function (PDF) cannot be identified to describe the uncertainty on the system parameters (sections 3.2); and (b) DOA's or the initial conditions that lead to these attractors (section 3.3). The computational time and storage savings are illustrated on a second order Duffing oscillator under harmonic forcing (section 4).

2. OVERVIEW OF CCMT [23, 24]

Consider the system

$$d\mathbf{x}/dt = \mathbf{f}(\mathbf{x}, \boldsymbol{\alpha}), \tag{1}$$

where $\mathbf{x}$ is a vector the elements of which are the dynamic system variables x_l ($l = 1, \ldots, L$), t is time, and $\boldsymbol{\alpha}$ is the system parameter vector. We will assume that the system is autonomous, i.e., the vector function $\mathbf{f}(\mathbf{x}, \boldsymbol{\alpha})$ does not explicitly depend on t. This assumption does not lead to loss of generality, since a non-autonomous system can be converted to an autonomous system by letting t be an additional dynamic variable.

In order to illustrate the philosophy of CCMT, first let $\boldsymbol{\alpha} = \boldsymbol{\alpha}_m$ be a fixed vector. Then, for every trajectory departure point $\mathbf{x}(t) = \mathbf{x}'$ in the state space, the arrival point at time $t + \tau$ can be uniquely determined from

$$\tilde{\mathbf{x}}(\mathbf{x}', \boldsymbol{\alpha}_m) = \int_t^{t+\tau} \mathbf{f}(\mathbf{x}(t'), \boldsymbol{\alpha}_m)\, dt' \tag{2}$$

by the numerical integration of equation (1). Now partition the state space region of interest, R, into cells V_j ($j = 1, \ldots, J$), each of which is a specified set of magnitude intervals for the dynamical variables. The region outside R is represented by a single cell V_{j+1}, out of which there is no transition (sink cell). The CCMT regards system evolution in time as a mapping between these cells. The mapping rules can be also interpreted as the conditional probability, $g_{j,j'}(\tau)$, of trajectory transition to V_j during the time interval $[t, t + \tau]$, given that the departure point is within $V_{j'}$ at time t. The time period τ is the mapping step. The cell to cell transition probabilities $g_{j,j'}(\tau)$ can be quantified using either simple cell mapping (SCM) or generalized cell mapping (GCM). For SCM, a single departure point is chosen in each cell $V_{j'}$ (usually the center) and the arrival point is determined from equation (2) to find the image cell. Since there is one departure point from $V_{j'}$ and the arrival point is uniquely determined from equation (2) once the departure point is specified, $g_{j,j'}(\tau) = 1$ if the arrival point is within V_j. Otherwise, $g_{j,j'}(\tau) = 0$. In SCM terminology, a cell is said to be a *periodic* cell of period K if it maps onto itself in K mapping steps (i.e., in time period $K\tau$). This definition implies that the sink cell is also a periodic cell with $K = 1$. If a cell is not periodic, then it is a *transient* cell. The GCM allows multiple departure points from cells. Subsequently a cell can have several image cells with GCM. In this case, two procedures proposed by Hsu [23] to find $g_{j,j'}(\tau)$ are as follows.

1. Find the portion of the volume of $V_{j'}$ that maps to V_j during $[t, t + \tau]$ using point to point mapping (i.e., from equation (2)) and define $g_{j,j'}(\tau)$ as the ratio of this volume to the total volume of $V_{j'}$.

2. Further partition each cell $V_{j'}$ into $I_{j'}$ equivolume subcells and choose one departure point in each subcell ("interior and boundary sampling"). If $\mathbf{x}'_{i,j'}$ ($i = 1, \ldots, I_{j'}$) is a point in the ith subcell of cell $V_{j'}$, then

$$g_{j,j'}(\tau) = N_{j,j'}(\boldsymbol{\alpha})/I_{j'}, \tag{3}$$

where $N_{j,j'}(\boldsymbol{\alpha})$ is the number of system trajectories arriving in cell V_j which have originated from cell V'_j for a given $\boldsymbol{\alpha}$, and is again determined by integrating equation (1) over $[t, t + \tau]$ with $\mathbf{x}(t) = [\mathbf{x}'_{1,j'}, \ldots, \mathbf{x}'_{I_{j'},j'}]^{\mathrm{T}}$.

In GCM terminology, a cell V_j *leads* to cell V_i if the k-step transition probability from V_j to V_i (i.e., the probability that $x(t + k\tau) \in V_i$, given that $x(t) \in V_j$) is positive. A cell V_i is said to *communicate with* cell V_j if and only if V_i leads to V_j and V_j leads to V_i. A cell V_i is called a *persistent* cell if the system, defined by equation (1) and starting from cell V_i, ultimately returns to V_i. Otherwise, V_i is a *transient* cell. The set of persistent cells that

communicate with each other form a *persistent group* (PG). Once the system (i.e., equation (1)) is in a PG it stays in that PG forever. A PG may correspond, for example, to an asymptotically stable stationary or periodic solution of the system. The set of cells that lead to one specific PG are called *single domicile* cell. The single domicile cells leading to a PG constitute the *basin of attraction* (BOA) for that PG. The BOA is the GCM terminology for DOA. The DOA and BOA will be used interchangeably in the rest of the paper. Cells that lead to more than one PG are called *multiple domicile cells*.

A SCM and a GCM are called *compatible* if, for every cell, the single image of the SCM is a member of the set of multiple images of GCM. For both SCM and GCM, $g_{j,J+1}(\tau) = 1$ if $j = J + 1$ and 0 otherwise, since V_{J+1} is sink cell by definition. In sections 2.1 and 2.2 it is shown how the $g_{j,j'}(\tau)$ are used to determine the PG's, the BOA's and their statistical properties.

2.1. DETERMINATION OF THE LIMITING PROBABILITY DISTRIBUTION OF PGS

Once the transition probabilities $g_{j,j'}(\tau)$ are found, the probability, $P_j(t + \tau)$, that the dynamic variables are within cell V_j ($j = 1, \ldots, J + 1$) at time $t + \tau$ is obtained from the relation

$$P_j(t + \tau) = \sum_{j'=1}^{J+1} g_{j,j'}(\tau) P_{j'}(t) \tag{4}$$

for a given $P_j(0)$. Since the system has to be at some point in the state space at any time and the V_j partition the state space, we must have

$$\sum_{j=1}^{J+1} P_j(t) = 1, \quad \text{for all } t; \qquad \sum_{j=1}^{J+1} g_{j,j'}(\tau) = 1, \quad \text{for all } j' = 1, \ldots, J + 1; \tag{5}$$

and thus equations (3) and (4) define a Markov chain in discrete time. Then

$$P_j^{\infty} \equiv \lim_{k \to \infty} P_j(k\tau) \tag{6}$$

yields the limiting probability distribution of the PG's [23] and hence information about the long-term behavior of the system. While equation (6) may not converge for PG's consisting of periodic cells, Hsu [23] shows how P_j^{∞} can be found for such a PG by decomposing the PG into subgroups. For fixed initial conditions and system parameters, τ / P_j^{∞} can be interpreted as the mean duration between trajectory visits to cell V_j [31]. The P_j^{∞} are also useful in determining the statistical properties of chaotic attractors. For example, the asymptotic mean value, $\bar{\mathbf{x}}$, of the location of the system in the state space can be found from

$$\bar{\mathbf{x}} = \sum_{j=1}^{J} \mathbf{x}_j P_j^{\infty}, \tag{7}$$

where $\mathbf{x}_j$ is a point within cell V_j. Similarly, the variance of the dynamic variable x_l from its mean value $\bar{x}_l$ can be found from

$$\sigma_l^2 = \sum_{j=1}^{J} (x_{lj} - \bar{x}_l)^2 P_j^{\infty}, \tag{8}$$

where x_{lj} and $\bar{x}_l$ are the lth components of the vectors $\mathbf{x}_j$ and $\bar{\mathbf{x}}$, respectively. When the system parameters are stochastic variables, then equation (3) is modified as

$$g_{j,j'}(\tau) = \sum_{m=1}^{M} \frac{N_{j,j'}(\boldsymbol{\alpha}_m)}{I_{j'}} \tilde{P}(\boldsymbol{\alpha}_m), \tag{9}$$

where $\boldsymbol{\alpha}_m$ ($m = 1, \ldots, M$) are a set of selected discrete values of the parameter vector and $\tilde{P}(\boldsymbol{\alpha}_m)$ are the associated probabilities determined from the given joint pdf for the system parameters [23, 29, 32]. Then the analysis is carried out as described above for fixed $\boldsymbol{\alpha}$ through equations (4)–(6). A third procedure proposed by Sun and Hsu [30] for the determination of $g_{j,j'}(\tau)$ is to approximate $P(\mathbf{x}, t+\tau|\mathbf{x}', t)$, the transition probability density from $\mathbf{x}'$ to $\mathbf{x}$ in the state space within $[t, t+\tau]$, by a some assumed distribution and determine the $g_{j,j'}(\tau)$ from

$$g_{j,j'}(\tau) = \int_{V_j} \mathrm{d}\mathbf{x} P(\mathbf{x}, t+\tau|\mathbf{x}_{j'}, t),$$

where $\mathbf{x}_{j'}$ denotes the center of cell $V_{j'}$ (see equation (5) of reference [30]). Compared to procedure 2, this procedure has been found to lead to substantial decrease in the computation time for the determination of $g_{j,j'}(\tau)$ for systems under external and parametric Gaussian white noise excitations.

2.2. DETERMINATION OF PGS, BOA'S AND THEIR ABSORPTION PROBABILITIES

In order to determine the PG's, the CCMT first selects a SCM compatible with given GCM for the system. Such an SCM can be selected by picking one among the multiple image cells of a cell V_j and regarding this image as the single image cell of V_j. Then, the mapping evolution of each cell in the selected SCM is followed to determine if the cell is periodic or transient. After having determined the periodic cells for the selected SCM, the search for the PG's starts by choosing a cell that is periodic under the selected SCM and following its mapping evolution while considering all the possible multiple images of the cell for the given GCM. This procedure generates several image sequences for the selected cell. If an image sequence leads to a cell that is known to be a transient cell or a persistent cell of a previously discovered PG, then all the cells in this sequence are tagged as transient. If the sequence leads to a new persistent cell, the sequence is continued to locate all the cells that the new persistent cell leads to. These cells are tagged as the members of the new PG. All the other cells in the sequence are tagged as transient. The tagging rules are based on some properties of finite Markov chains given in reference [23].

In order to locate the domiciles of the transient cells (i.e., the PGs that the transient cells lead to) a pre-image array is constructed for the cells in the PG's. A pre-image cell of a cell V_j is a cell which has V_j as one of its images. Since the domicile of a transient cell is also the domicile of all its pre-image cells, the pre-image array is used to march backwards to locate the cells that have their domiciles as the PG under consideration. The transient cells can be single domicile cells (i.e., leading to only one PG) or multiple domicile cells (i.e., leading to more than one PG). As indicated before, single domicile cells constitute BOA's. Multiple domicile cells delineate the boundaries of the BOA's.

Once all the PG cells are determined and the BOA's consisting of single domicile cells are identified, the absorption probabilities of multiple domicile transient cells in a given PG are calculated. For this purpose, the cell space has to be rearranged in such a way that persistent cells are listed first, followed by the transient cells. A subsequent simultaneous rearrangement of rows and columns of the transition probability matrix $\mathbf{M}$, the elements of which consist of the $g_{j,j'}(\tau)$ obtained from GCM, leads to the normal form of $\mathbf{M}$, given by

$$\mathbf{M} = \begin{bmatrix} \mathbf{M}' & \mathbf{T} \\ \boldsymbol{\Theta} & \mathbf{Q} \end{bmatrix},$$

where $\boldsymbol{\Theta}$ is a null matrix and the submatrices $\mathbf{M}'$, $\mathbf{T}$ and $\mathbf{Q}$ describe, respectively, the transitions: (a) between persistent cells; (b) from transient to persistent cells; and (c) from

transient to transient cells. Then it can be shown [33] that the absorption probability of a multiple domicile transient cell V_j in a persistent cell V_i is the element (i, j) of the matrix $\mathbf{A} = \mathbf{T}(\mathbf{I} - \mathbf{Q})^{-1}$, where $\mathbf{I}$ is the identity matrix.

3. DEVELOPMENT OF THE NEW ALGORITHMS

The new algorithms (sections 3.2 and 3.3) are similar in spirit to the approach developed by Sun and Hsu [30] to reduce the computational time in the global analysis of nonlinear random vibrations using CCMT. The theoretical basis for the algorithms is described in section 3.1.

3.1. THEORETICAL BASIS FOR THE ALGORITHMS

Assume that the changes in the dynamic system variables and system parameters are statistically independent and that the pdf for the system parameters, $P(\boldsymbol{\alpha})$. is given. The assumption of statistical independence includes, for example, random fluctuations of the system parameters around some mean value, but excludes the situations which the magnitude of the fluctuations may be influenced by the changes in the dynamical variables. If the system parameters are fixed at $\boldsymbol{\alpha}_m$, then $P(\boldsymbol{\alpha}) = \delta(\boldsymbol{\alpha} - \boldsymbol{\alpha}_m)$, where $\delta(\cdot)$ denotes the Dirac delta function. Subsequently, the probability that the system is within a small volume element $\mathrm{d}\boldsymbol{\alpha}\,\mathrm{d}\mathbf{x}$ around a specified point $\{\boldsymbol{\alpha}, \mathbf{x}\}$ in the product space $\mathbf{x} \times \boldsymbol{\alpha}$ at time $t + \mathrm{d}t$, $P(\mathbf{x}, \boldsymbol{\alpha}, t + \tau)\,\mathrm{d}\boldsymbol{\alpha}\,\mathrm{d}\mathbf{x}$, can be determined from equation (2) with given $\boldsymbol{\alpha}(t)$, $P(\boldsymbol{\alpha})$ and $\mathbf{x}(t)$, which implies that the system under consideration has the *Markov Property* in $\mathbf{x} \times \boldsymbol{\alpha}$. The Markov Property can be expressed through the Chapman–Kolmogorov equation [35] as

$$P(\mathbf{x}, \boldsymbol{\alpha}, w|\mathbf{x}'', \boldsymbol{\alpha}'', u) = \int \mathrm{d}\boldsymbol{\alpha}' \int \mathrm{d}\mathbf{x}' P(\mathbf{x}, \boldsymbol{\alpha}, w|\mathbf{x}', \boldsymbol{\alpha}', v) P(\mathbf{x}', \boldsymbol{\alpha}', v|\mathbf{x}'', \boldsymbol{\alpha}'', u), \qquad 0 \leqslant u \leqslant v \leqslant w, \tag{10}$$

where u, v and w denote time and $P(A|B)$ denotes the conditional probability that event set A occurs given that event set B occurs (i.e., the transition probability from event set B to event set A). Note that since the event space under consideration (i.e., the space of all possible sets of events $\{\mathbf{x}, \boldsymbol{\alpha}, t\}$) is continuous, all the conditional probabilities in equation (10) are per unit volume of the event space.

Now replace w and v in equation (10) with $t + \tau$ and t, respectively, to obtain

$$P(\mathbf{x}, \boldsymbol{\alpha}, t + \tau|\mathbf{x}'', \boldsymbol{\alpha}'', u) = \int \mathrm{d}\boldsymbol{\alpha}' \int \mathrm{d}\mathbf{x}' P(\mathbf{x}, \boldsymbol{\alpha}, t + \tau|\mathbf{x}', \boldsymbol{\alpha}', t) P(\mathbf{x}', \boldsymbol{\alpha}', t|\mathbf{x}'', \boldsymbol{\alpha}'', u), \qquad 0 \leqslant u \leqslant t \leqslant t + \tau. \tag{11}$$

Integrating equation (11) over all possible $0 \leqslant u \leqslant t$, $\mathbf{x}''$ and $\boldsymbol{\alpha}''$, we obtain

$$P(\mathbf{x}, \boldsymbol{\alpha}, t + \tau) = \int \mathrm{d}\boldsymbol{\alpha}' \int \mathrm{d}\mathbf{x}' P(\mathbf{x}, \boldsymbol{\alpha}, t + \tau|\mathbf{x}', \boldsymbol{\alpha}', t) P(\mathbf{x}', \boldsymbol{\alpha}', t), \tag{12}$$

which yields the continuous counterpart of equation (5) as

$$\int \mathrm{d}\boldsymbol{\alpha} \int \mathrm{d}\mathbf{x} P(\mathbf{x}, \boldsymbol{\alpha}, t) = 1, \quad \int \mathrm{d}\boldsymbol{\alpha} \int \mathrm{d}\mathbf{x} P(\mathbf{x}, \boldsymbol{\alpha}, t|\mathbf{x}', \boldsymbol{\alpha}', t') = 1, \qquad t' \leqslant t. \tag{13}$$

From the given $P(\boldsymbol{\alpha})$ and assumption of statistical independence of the variations in dynamic variables and system parameters,

$$P(\mathbf{x}, \boldsymbol{\alpha}, t+\tau|\mathbf{x}', \boldsymbol{\alpha}', t) = P(\mathbf{x}, t+\tau|\mathbf{x}', \boldsymbol{\alpha}', t)P(\boldsymbol{\alpha}, t+\tau|\mathbf{x}', \boldsymbol{\alpha}', t), \tag{14}$$

and

$$P(\mathbf{x}, \boldsymbol{\alpha}, t) = P(\mathbf{x}, t)P(\boldsymbol{\alpha}). \tag{15}$$

Also, once $\mathbf{x}(t)$ and $\boldsymbol{\alpha}(t)$ are specified, the location of the dynamic variables in the state space at $t+\tau$ is uniquely determined from equation (2) and, subsequently,

$$P(\mathbf{x}, t+\tau|\mathbf{x}', \boldsymbol{\alpha}', t) = \delta(\mathbf{x} - \tilde{\mathbf{x}}(\mathbf{x}', \boldsymbol{\alpha}')), \tag{16}$$

where

$$\tilde{\mathbf{x}}(\mathbf{x}', \boldsymbol{\alpha}') = \int_t^{t+\tau} \mathbf{f}(\mathbf{x}(t'), \boldsymbol{\alpha}')\, \mathrm{d}t' \tag{17}$$

is obtained from the numerical integration of equation (1) with $\mathbf{x}(t) = \mathbf{x}'$ and fixed $\boldsymbol{\alpha} = \boldsymbol{\alpha}'$, as in equation (2). The substitution of equations (14)–(16) into equation (12) and integration over all possible $\boldsymbol{\alpha}$ yields

$$P(\mathbf{x}, t+\tau) = \int \mathrm{d}\boldsymbol{\alpha}' \int \mathrm{d}\mathbf{x}' \delta(\mathbf{x} - \tilde{\mathbf{x}}(\mathbf{x}', \boldsymbol{\alpha}'))P(\boldsymbol{\alpha}')P(\mathbf{x}', t). \tag{18}$$

In order to find the cell to cell transition probabilities, partition the state space region of interest for the analysis (i.e., R) into computational cells V_j ($j = 1, \ldots, J$), and let V_{j+1} be the sink cell as before. Then approximate $P(\mathbf{x}, t)$ as

$$P(\mathbf{x}, t) = \sum_{j=1}^{J} \frac{P_j(t)e_j(\mathbf{x})}{v_j}, \qquad e_j(\mathbf{x}) \equiv \begin{cases} 1, & \text{if } \mathbf{x} \in V_j \\ 0, & \text{otherwise} \end{cases}, \qquad P_j(t) \equiv \int_{V_j} \mathrm{d}\mathbf{x} P(\mathbf{x}, t), \tag{19}$$

where v_j is the volume of the cell V_j. Since $P_j(t)$ ($j = 1, \ldots, J$) is the probability that $\mathbf{x}(t)$ is within V_j by definition, equation (19) assumes that the location of the dynamical variables within a cell V_j is uniformly distributed over that cell at all times. Substitution of equation (19) into equation (18) and integration over V_j yields

$$P_j(t+\tau) = \sum_{j'=1}^{J+1} g_{j,j'}(\tau)P_{j'}(t), \tag{20}$$

where

$$g_{i,j'}(\tau) = \begin{cases} \dfrac{1}{v_{j'}} \displaystyle\int \mathrm{d}\boldsymbol{\alpha}' \int_{V_{j'}} \mathrm{d}\mathbf{x}' e_j(\tilde{\mathbf{x}}(\mathbf{x}', \boldsymbol{\alpha}'))P(\boldsymbol{\alpha}'). & \text{if } V_{j'} \in R, \\ 1, & \text{if } j' = j = J+1, \\ 0, & \text{if } j' = J+1 \quad \text{and} \quad j \neq J+1, \end{cases} \tag{21}$$

and the function $e_j(\mathbf{x})$ is as defined in equation (19).

The main differences between the approach described above and the approach of Sun and Hsu [30] are that: (a) the theoretical development in reference [30] starts from equation (12) rather than equation (10); and (b) reference [30] additionally assumes that $p(\mathbf{x}, \tau|\mathbf{x}_0, \tau)$ is a Gaussian. Also, the $\boldsymbol{\alpha}$ dependence of the system evolution is implicit in the approach of reference [30]. The algorithms described in section 3.2 and 3.3 originate from these differences. Regarding the correspondence of the above approach to the procedures described in section 2, procedure 1 in section 2 approximates equation (21) for fixed $\boldsymbol{\alpha}$ by finding the region in $V_{j'}$ for which $e_j(\tilde{\mathbf{x}}(\mathbf{x}', \boldsymbol{\alpha}')) = 1$. Also, since both $1/I_{j'}$ in equation (3) and $\mathrm{d}\mathbf{x}'/v_{j'}$ in equation (21) can be interpreted as the probability distributions of the

dynamical variables within $V_{j'}$ under the assumption of uniform distribution, procedure 2 in section 2 (i.e., the interior and boundary sampling process) or equation (3) is equivalent to a Monte Carlo scheme to approximate the integral over $V_{j'}$ in equation (21). Again, since equation (9) can be regarded as the extension of the Monte Carlo approach of procedure 2 to the system parameter space, the simplest interpretation of $\tilde{P}(\boldsymbol{\alpha}_m)$ $(m = 1, \ldots, M)$ in equation (9) is that $\tilde{P}(\boldsymbol{\alpha}_m) = 1/M$, with $\boldsymbol{\alpha}_m$ selected by sampling over $P(\boldsymbol{\alpha})$. Other possible ways of selecting $\boldsymbol{\alpha}_m$ for the Monte Carlo evaluation of the integral in equation (21) over the parameter space, corresponding interpretations of $\tilde{P}(\boldsymbol{\alpha}_m)$ and a discussion of the associated error magnitudes can be found in reference [36]. If $\boldsymbol{\alpha}_m$ are chosen independent of $P(\boldsymbol{\alpha})$, then the integral in over the parameter space in equation (21) is being evaluated by quadratures rather than Monte Carlo techniques, which carries the assumption that each $\boldsymbol{\alpha}_m$ is uniformly distributed within some region of the system parameter space and $\tilde{P}(\boldsymbol{\alpha}_m)$ needs to be interpreted as the integral of $P(\boldsymbol{\alpha})$ over these regions (see section 3.2).

3.2. DETERMINING THE LIMITING PROBABILITY DISTRIBUTION OF PG'S

It will be shown later, in section 4, that the determination of the trajectory arrival points from equation (2) towards the computation of $g_{j,j'}(\tau)$ can account for 96% of the total computational time spent in determining the PG's and their probability distributions and 41% of the total time for the global analysis. If the integral in equation (21) over the parameter space is evaluated using a Monte Carlo scheme (e.g., using equation (9)), then the $g_{j,j'}(\tau)$ need to be recomputed every time $P(\boldsymbol{\alpha})$ is changed. This recomputation process can be avoided by using the following quadrature scheme.

In an analogous manner to equation (19), partition the system parameter space into M cells $\tilde{V}_m$ $(m = 1, \ldots, M)$ and approximate $P(\boldsymbol{\alpha})$ by a set of piecewise constant functions as

$$P(\boldsymbol{\alpha}) = \sum_{m=1}^{M} \frac{\tilde{P}_m e_m(\boldsymbol{\alpha})}{\tilde{v}_m}, \qquad e_m(\boldsymbol{\alpha}) = \begin{cases} 1, & \text{if } \boldsymbol{\alpha} \in \tilde{V}_m \\ 0, & \text{otherwise,} \end{cases} \qquad \tilde{P}_m \equiv \int_{V_m} \mathrm{d}\boldsymbol{\alpha} P(\boldsymbol{\alpha}), \tag{22}$$

where $\tilde{v}_m$ is the volume of the cell $\tilde{V}_m$. Equations (20), (21) and (22) show that

$$P_j(t + \tau) = \sum_{j'=1}^{J+1} \sum_{m=1}^{M} \tilde{g}_{j,j',m}(\tau) \tilde{P}_m P_{j'}(t), \tag{23}$$

where now the cell to cell transition probabilities are defined separately for each fixed $\boldsymbol{\alpha}_m \in \tilde{V}_m$ as

$$\tilde{g}_{i,j'm}(\tau) = \begin{cases} \dfrac{1}{v_j'} \displaystyle\int_{V_{j'}} \mathrm{d}\mathbf{x}'\, e_j(\tilde{\mathbf{x}}(\mathbf{x}', \boldsymbol{\alpha}_m)), & \textit{if } V_{j'} \in R, \\ 1, & \text{if } j' = j = \mathrm{J} + 1, \\ 0, & \text{if } j' = J + 1 \quad \textit{and} \quad i \neq J + 1 \end{cases} \tag{24}$$

Since $\boldsymbol{\alpha}_m$ are fixed and hence independent of the choice of $P(\boldsymbol{\alpha})$, equation (23) can be alternatively expressed as

$$P_{j,m}(t + \tau) = \sum_{j'=1}^{J+1} \tilde{g}_{j,j',m}(\tau) P_{j',m}(t), \qquad P_j(t) = \sum_{m=1}^{M} \tilde{P}_m P_{j,m}(t). \tag{25, 26}$$

Then, the transition probabilities $\tilde{g}_{j,j',m}(\tau)$ need to be calculated only once to find $P_{j,m}(k\tau)$ $(k = 0, 1, 2, \ldots)$ iteratively from equation (25) and these $P_{j,m}(k\tau)$ can be used with $\tilde{P}_m$ corresponding to different $P(\boldsymbol{\alpha})$ to find $P_j(t)$ from equation (26). As before, P_j^{∞} (see

equation (6)) yields the probability distribution of PG's, and the results can be improved by the increasing number of $\tilde{V}_m$ used to partition the system parameter space.

In principle, all the non-zero P_j^∞ obtained from equations (25) and (26) correspond to persistent cells. On the other hand, some transient cells may be inadvertently included in the predicted PG structure, since only a finite number of iterations (i.e., k) can be used to approximate P_j^∞ from equations (25) and (26). For example, if the convergence criterion (or the stopping rule) is

$$\max_j \frac{|P_{j,m}(k\tau) - P_{j,m}((k-1)\tau)|}{P_{j,m}(k\tau)} \leqslant \varepsilon_1, \tag{27}$$

where ε_1 is a specified small number, a transient cell V_j may satisfy the criterion if it takes a long time (i.e., many τ's) for a trajectory starting from this cell to be absorbed in a persistent group, depending on how small ε_1 is. This problem is not relevant to the implementation of the CCMT as described in section 2.2, since the persistent and transient cells are determined by starting from a cell that is periodic under a selected SCM compatible with the given GCM and following its mapping evolution while considering all the possible multiple images of the cell for the given GCM. However, the problem can be eliminated by comparing the approximate mean trajectory return times for the cells (i.e., $r_j = \tau/P_{j,m}(k\tau)$) to the maximum return time. Since a trajectory starting from a subcell of cell V_j (which has a total of I_j subcells) can at most visit all the other subcells in R before returning to the same subcell, this maximum return time is

$$r_{max} = \tau \sum_{j=1}^{J} I_j. \tag{28}$$

Subsequently, if $r_j > r_{max}$ (or $P_{j,m}(k) < 1/\sum_{j=1}^{J} I_j$), then V_j is a transient cell. A few transient cells may still remain within the predicted PG's due to numerical round-off even after the application of this criterion, but such cells can be eliminated during the determination of BOA's and their absorption probabilities, as described in the next section.

3.3. DETERMINATION OF PG'S, BOA'S AND ABSORPTION PROBABILITIES

For the determination of the PG's, the new algorithm also follows the mapping evolution of the cells (section 2.2). The main difference is that the new algorithm does not use SCM to determine the starting set of cells towards the identification of the PG's, since the persistent cells are identified earlier as described in section 3.2.

For the determination of BOA's and their absorption probabilities, the new algorithm uses the k-step transition probabilities, $\tilde{\rho}_{j,i,m}(k+1)$, from V_i to V_j for fixed $\boldsymbol{\alpha}_m$ instead of pre-image arrays and the matrix $\mathbf{A} = \mathbf{T}(\mathbf{I} - \mathbf{Q})^{-1}$ (section 2.2). A recurrence relationship for these probabilities can be obtained by: (1) letting $w = u + (k+1)\tau$, $v = u + \tau$ and $\boldsymbol{\alpha} = \boldsymbol{\alpha}_m$ in equation (10); and (2) proceeding in an analogous manner to the procedure outlined by equations (14)–(21) to obtain

$$\tilde{\rho}_{j,i,m}(k+1) = \sum_{j'=1}^{J+1} \tilde{g}_{j',i,m}(\tau)\tilde{\rho}_{j,j',m}(k), \tag{29}$$

where $\tilde{g}_{j',i,m}(\tau)$ is as given by equation (24). Then if γ indicates a PG, equation (29) shows that

$$\rho_{\gamma,i,m}(k+1) \equiv \sum_{j\in\gamma} \tilde{\rho}_{j,i,m}(k+1) = \sum_{j'=1}^{J+1} \tilde{g}_{j',i,m}(\tau)\rho_{\gamma,j',m}(k), \tag{30}$$

and subsequently, for fixed $\boldsymbol{\alpha}_m$, the absorption probability of trajectories starting from cell V_i in PG γ is

$$\rho^{\infty}_{\gamma,i,m} = \lim_{k\to\infty} \rho_{\gamma,i,m}(k). \tag{31}$$

To determine $\rho^{\infty}_{\gamma,i,m}$, the iterations with equation (30) are carried out until

$$\frac{|\rho_{\gamma,i,m}(k+1) - \rho_{\gamma,i,m}(k)|}{\rho_{\gamma,i,m}(k+1)} < \varepsilon_2 \tag{32}$$

for every i, where ε_2 is some specified small number, and then $\rho^{\infty}_{\gamma,i,m}$ is set to be equal to $\rho_{\gamma,i,m}(k+1)$. If $\rho^{\infty}_{\gamma,i,m}$ is non-zero for a cell V_i, then PG γ is a domicile of V_i. For single domicile transient cells, $\rho^{\infty}_{\gamma,i,m}$ is either 1 or 0. If $\rho^{\infty}_{\gamma,i,m} = 1$ (or, more precisely, $\rho^{\infty}_{\gamma,i,m} \geqslant 1 - \varepsilon_3$, where ε_3 is again a small specified number to account for numerical round-off), the cell V_i is a member of the BOA for PG γ. If V_i is a multiple domicile transient cell, then $\rho^{\infty}_{\gamma,i,m}$ is a number between 0 and 1, and indicates the absorption probability of trajectories starting from cell V_i in the PG γ. If there is uncertainty on $\boldsymbol{\alpha}$ represented by a given $P(\boldsymbol{\alpha})$, then the absorption probability of V_i in PG γ is

$$\rho^{\infty}_{\gamma,i} = \sum_{m=1}^{M} \rho^{\infty}_{\gamma,i,m} \tilde{P}_m, \tag{33}$$

where $\tilde{P}_m$ is as defined in equation (22).

4. ILLUSTRATION

The example system chosen to illustrate the computational efficiency of the new procedures presented in sections 3.2 and 3.3 is the second order forced Duffing oscillator under harmonic forcing used by Hsu [23] and Hsu and Chiu [37], i.e.,

$$\frac{\mathrm{d}^2x}{\mathrm{d}t^2} + \alpha_1 \frac{\mathrm{d}x}{\mathrm{d}t} + \alpha_2 x + x^3 = B\cos(t) \tag{34}$$

or

$$\mathrm{d}x_1/\mathrm{d}t = x_2, \qquad \mathrm{d}x_2/\mathrm{d}t = B\cos(t) - (\alpha_1 x_2 + \alpha_2 x_1 + x_1^3), \tag{35}$$

where x_1 and x_2 are the normalized displacement and velocity, respectively (i.e., dynamic variables) and α_1 and α_2 are the system parameters. Hsu [23] shows that for $\alpha_1 = 0{\cdot}25$, $\alpha_2 = 0{\cdot}02$ and $B = 8{\cdot}5$, the PG's of the system of equation (35) consist of: (a) three points corresponding to a third order subharmonic; and (b) a strange attractor.

For the purposes of illustration, α_1 and B in equation (35) were fixed as $\alpha_1 = 0{\cdot}25$ and $B = 8{\cdot}5$, and the following two cases were considered.

Case 1. α_2 is uniformly distributed over $0{\cdot}005 \leqslant \alpha_2 \leqslant 0{\cdot}035$, i.e.,

$$P(\alpha_2) = \begin{cases} \dfrac{1}{0{\cdot}035 - 0{\cdot}005}, & \text{if } 0{\cdot}005 \leqslant \alpha_2 \leqslant 0{\cdot}035, \\ 0, & \text{otherwise.} \end{cases} \tag{36}$$

Case 2. α_2 is normally distributed over $0{\cdot}005 \leqslant \alpha_2 \leqslant 0{\cdot}035$, with mean value $\alpha_2 = 0{\cdot}02$ and 90% confidence, which corresponds to a standard deviation of 0·00912 around this mean value, i.e.,

$$P(\alpha_2) = \frac{\mathrm{e}^{-(\alpha_2 - 0{\cdot}02)^2/2(0{\cdot}00912)^2}}{0{\cdot}00912(2\pi)^{1/2}}. \tag{37}$$

The region of interest in the state space for the analysis (i.e., R) was chosen to be $\{1{\cdot}5 \leqslant x_1 \leqslant 4{\cdot}2, -3 \leqslant x_2 \leqslant 6\}$ as in reference [23] and $150 \times 150 = 22\,500$ uniform sized cells (i.e., V_j) were used to partition R (also as in reference [23]). For both Cases 1 and 2 above, the uncertainty range for α_2 was partitioned using three cells (i.e., $\tilde{V}_m$). In Table 1 is shown the definition of $\tilde{V}_m$, including other data (i.e., $\alpha_{2,m}$, $\tilde{v}_m$ and $\tilde{P}_m$) needed for equations (22), (24) and (26). Since, by definition,

$$\tilde{P}_m = \frac{1}{\tilde{v}_m} \int_{V_m} \mathrm{d}\alpha_2 P(\alpha_2), \tag{38}$$

the $\tilde{P}_m$ in Table 1 were found from equations (36) and (37) by integrating $P(\alpha_2)$ over the respective α_2 ranges given in Table 1. The transition probabilities $\tilde{g}_{j,j',m}(\tau)$ in equation (24) were determined by: (1) using $\tau = 2\pi$ to obtain a cell to cell mapping that is stationary in time (since $B\cos(t) = B\cos(t+\tau)$): (2) using a fourth order Runge–Kutta scheme for the integration of equation (35) over $[t, t+\tau]$ with an internal time step size of $2\pi/60$ to find the $\tilde{\mathbf{x}}(x', \alpha_{2m})$ defined in equation (17) with $\alpha_{2,m,}$ as given in Table 1; and (3) dividing each cell V_j ($j = 1, \ldots, J = 22\,500$) into nine uniform subcells and choosing the departure point $\mathbf{x}' = [x_1 \;\; x_2]^{\mathrm{T}}$ to be the mid-point of each subcell to approximate the integral in equation (24).

In Figures 1–3 is shown the probability distribution of the PG's of the example system for $\alpha_2 = 0{\cdot}01$, $0{\cdot}02$ and $0{\cdot}03$, respectively, when $\alpha_1 = 0{\cdot}25$ and $B = 8{\cdot}5$ in equation (34). The data of Figures 1–3 were obtained from equation (25) recursively using the convergence criterion $\varepsilon_1 = 0{\cdot}001$ in equation (27) for all $j = 1, \ldots, J+1 = 22\,501$ (in about 120–150 iterations). It is shown in Figures 1–3 that while there is little change in the overall shape of the PG's with changing α_2 (compare regions marked "3" in Figures 1–3 and also regions marked "1" and "4"), the limiting probability distribution of the PG's can change substantially. For example, comparison of the regions marked "2" in Figures 1 and 2 shows that there is a two orders of magnitude change in P_j^{∞} of some cells in this region. The change increases to three orders of magnitude with increasing α_2 (compare regions marked "2" in Figures 1 and 3).

Figures 4 and 5 correspond to Cases 1 and 2 above, respectively. In these figures it is shown that, for the $P(\alpha_2)$ considered in this illustration (i.e., equation (36) and (37)), there is virtually no change in the PG structure with changing $P(\alpha_2)$ and a small change in the P_j^{∞} for some j (compare regions marked "2" in Figures 4 and 5, and also regions marked "5"). The maximum difference between the P_j^{∞} in Figures 4 and 5 is 32%. However, a comparison of Figures 1–5 indicates that there is a "fattening" of PG's with uncertainty on system parameters (e.g., compare regions marked "3" in Figures 1 and 4), as expected from previous applications of CCMT to systems with stochastic parameters (see, e.g., Chiu and Hsu [29]). The data for Figures 4 and 5 were obtained from the Figures 1–3 data and $\tilde{P}_m$ data in Table 1, using equation (26). In Table 2 are given some statistical properties of the asymptotic system behavior for Cases 1 and 2 which may be also used to assess the

TABLE 1

The definition of $\tilde{V}_m$ and the corresponding data for equations (22), (24) *and* (26)

Cell or data type	$m = 1$	$m = 2$	$m = 3$
$\tilde{V}_m$	$0{\cdot}005 \leqslant \alpha_2 \leqslant 0{\cdot}015$	$0{\cdot}015 \leqslant \alpha_2 \leqslant 0{\cdot}025$	$0{\cdot}025 \leqslant \alpha_2 \leqslant 0{\cdot}035$
$\alpha_{2,m}$	$0{\cdot}01$	$0{\cdot}02$	$0{\cdot}03$
$\tilde{v}_m$	$0{\cdot}015-0{\cdot}005 = 0{\cdot}01$	$0{\cdot}025-0{\cdot}015 = 0{\cdot}01$	$0{\cdot}035-0{\cdot}025 = 0{\cdot}01$
$\tilde{P}_m$ from equations (36) and (38)	$1/3$	$1/3$	$1/3$
$\tilde{P}_m$ from equations (37) and (38)	$0{\cdot}269$	$0{\cdot}462$	$0{\cdot}269$

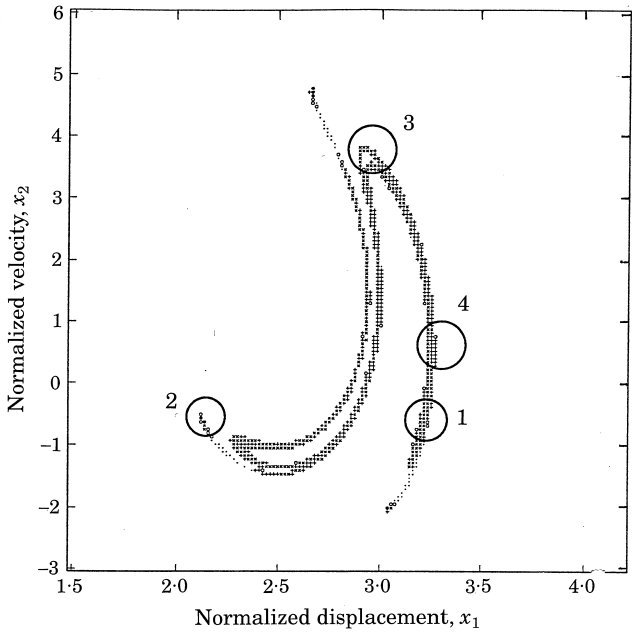

Figure 1. The probability distribution (P_i^∞) of the persistent groups for the example system and for $\alpha_2 = 0{\cdot}01$. ●, $1{\cdot}0 \times 10^{-2} \leqslant P_i^\infty \leqslant 1{\cdot}0 \times 10^{-1}$; ×, $1{\cdot}0 \times 10^{-3} \leqslant P_i^\infty \leqslant 1{\cdot}0 \times 10^{-2}$; +, $1{\cdot}0 \times 10^{-4} \leqslant P_i^\infty \leqslant 1{\cdot}0 \times 10^{-3}$; ○, $1{\cdot}0 \times 10^{-5} \leqslant P_i^\infty \leqslant 1{\cdot}0 \times 10^{-4}$; ·, $1{\cdot}0 \times 10^{-6} \leqslant P_i^\infty \leqslant 1{\cdot}0 \times 10^{-5}$.

impact of the choice of the PDF for α_2 on the structure of PG's. The data in Table 2 were obtained by using the Figures 4 and 5 data in conjunction with equations (7) and (8).

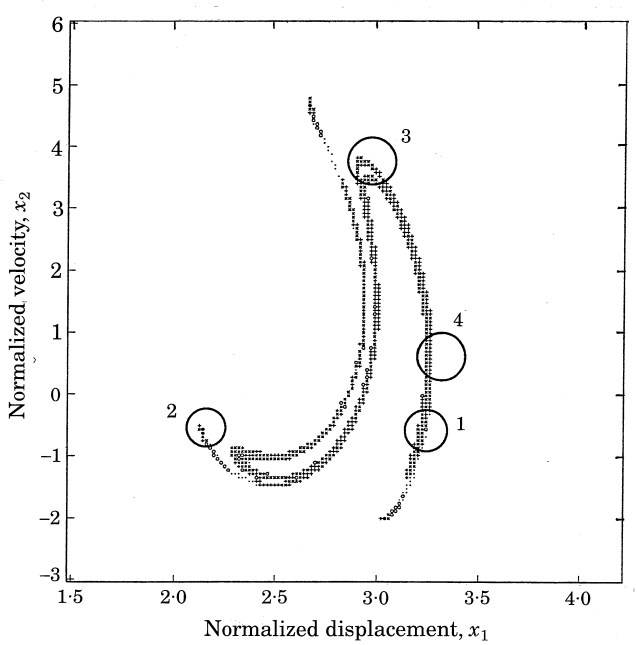

Figure 2. The probability distribution (P_i^∞) of the persistent groups for the example system and for $\alpha_2 = 0{\cdot}02$. ●, $1{\cdot}0 \times 10^{-2} \leqslant P_i^\infty \leqslant 1{\cdot}0 \times 10^{-1}$; ×, $1{\cdot}0 \times 10^{-3} \leqslant P_i^\infty \leqslant 1{\cdot}0 \times 10^{-2}$; +, $1{\cdot}0 \times 10^{-4} \leqslant P_i^\infty \leqslant 1{\cdot}0 \times 10^{-3}$; ○, $1{\cdot}0 \times 10^{-5} \leqslant P_i^\infty \leqslant 1{\cdot}0 \times 10^{-4}$; ·, $1{\cdot}0 \times 10^{-6} \leqslant P_i^\infty \leqslant 1{\cdot}0 \times 10^{-5}$.

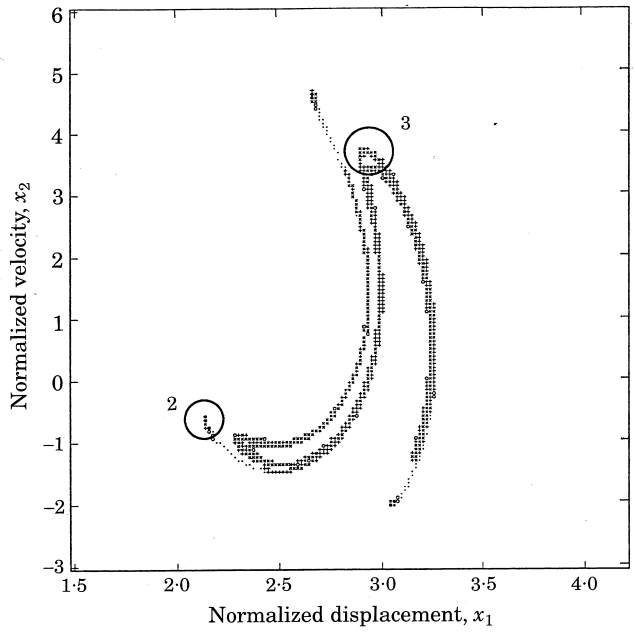

Figure 3. The probability distribution (P_i^∞) of the persistent groups for the example system and for $\alpha_3 = 0{\cdot}03$. ●, $1{\cdot}0 \times 10^{-2} \leqslant P_i^\infty \leqslant 1{\cdot}0 \times 10^{-1}$; ×, $1{\cdot}0 \times 10^{-3} \leqslant P_i^\infty \leqslant 1{\cdot}0 \times 10^{-2}$; +, $1{\cdot}0 \times 10^{-4} \leqslant P_i^\infty \leqslant 1{\cdot}0 \times 10^{-3}$; ○, $1{\cdot}0 \times 10^{-5} \leqslant P_i^\infty \leqslant 1{\cdot}0 \times 10^{-4}$; ·, $1{\cdot}0 \times 10^{-6} \leqslant P_i^\infty \leqslant 1{\cdot}0 \times 10^{-5}$.

In Figure 6 are shown the PG's for $\alpha_2 = 0{\cdot}02$, which are obtained by the procedure described in section 3.3. This α_2 value is the one considered in reference [23]. Comparison of Figure 6 with Figures 1–3 illustrates the discussion in section 3.2 as to how transient

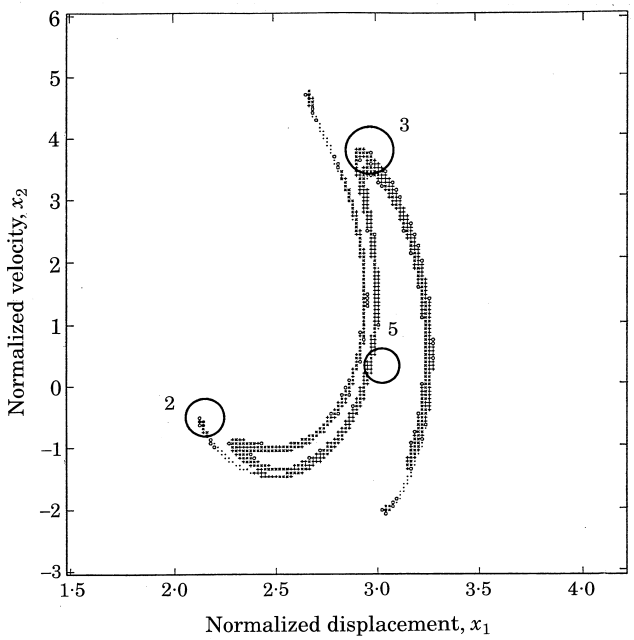

Figure 4. The probability distribution (P_i^∞) of the persistent groups for the example system and for α_2 uniformly distributed (Case 1). ●, $1{\cdot}0 \times 10^{-2} \leqslant P_i^\infty \leqslant 1{\cdot}0 \times 10^{-1}$; ×, $1{\cdot}0 \times 10^{-3} \leqslant P_i^\infty \leqslant 1{\cdot}0 \times 10^{-2}$; +, $1{\cdot}0 \times 10^{-4} \leqslant P_i^\infty \leqslant 1{\cdot}0 \times 10^{-3}$; ○, $1{\cdot}0 \times 10^{-5} \leqslant P_i^\infty \leqslant 1{\cdot}0 \times 10^{-4}$; ·, $1{\cdot}0 \times 10^{-6} \leqslant P_i^\infty \leqslant 1{\cdot}0 \times 10^{-5}$.

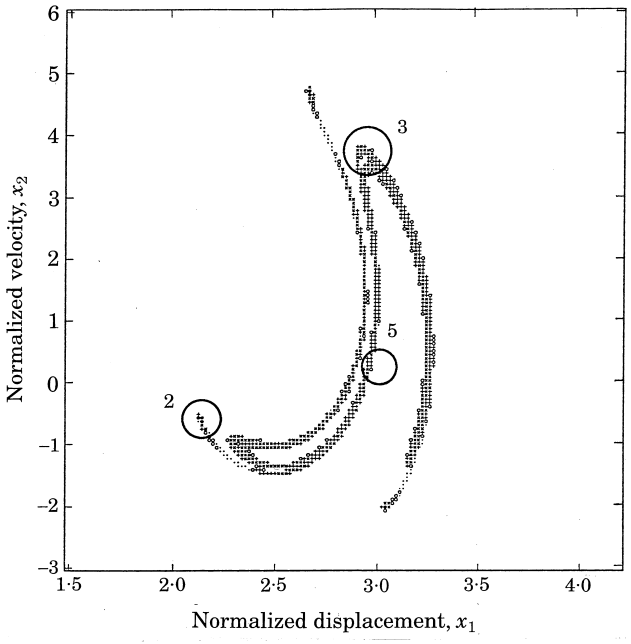

Figure 5. The probability distribution (P_i^∞) of the persistent groups for the example system and for α_2 normally distributed (Case 2). ●, $1{\cdot}0 \times 10^{-2} \leqslant P_i^\infty \leqslant 1{\cdot}0 \times 10^{-1}$; ×, $1{\cdot}0 \times 10^{-3} \leqslant P_i^\infty \leqslant 1{\cdot}0 \times 10^{-2}$; +, $1{\cdot}0 \times 10^{-4} \leqslant P_i^\infty \leqslant 1{\cdot}0 \times 10^{-3}$; ○, $1{\cdot}0 \times 10^{-5} \leqslant P_i^\infty \leqslant 1{\cdot}0 \times 10^{-4}$; ·, $1{\cdot}0 \times 10^{-6} \leqslant P_i^\infty \leqslant 1{\cdot}0 \times 10^{-5}$.

cells may appear as part of the PG's depending on the convergence criterion (i.e., equation (27)). In Figures 7(a)–(d) are shown the BOA's, the absorption probabilities of the multiple domicile cells into the sink cell, the third subharmonic group and the strange (chaotic) attractor, respectively, for $\alpha_2 = 0{\cdot}02$. The absorption probabilities and the BOA's are determined using the convergence criteria given in section 3.3, with $\varepsilon_2 = 0{\cdot}0001$ and $\varepsilon_3 = 0{\cdot}01$. The PG's shown in Figure 6, BOA shown in Figure 7(a) and the absorption probabilities for the multiple domicile cells shown in Figures 7(b)–(d) are identical to those given in reference [23]. This agreement is important for the benchmarking of the new algorithms.

Comparison of Figures 7(a) and 8 illustrates the change in the structure of the BOA's with changing α_2 (i.e., from $\alpha_2 = 0{\cdot}02$ to $\alpha_2 = 0{\cdot}01$). Some multiple domicile cells between the BOA's for the third order subharmonic group and the strange attractor become part of the BOA for the third order subharmonic group (compare the regions marked "1" in Figures 7(a) and 8), the multiple domicile cell region

TABLE 2

Some statistical properties of the example system asymptotic behavior, for $\alpha_1 = 0{\cdot}25$, $B = 8{\cdot}5$ *and* $0{\cdot}005 \leqslant \alpha_2 \leqslant 0{\cdot}035$

Statistical property†	$P(\alpha_2)$ from equation (36)	$P(\alpha_2)$ from equation (37)
$\bar{x}_1$	2·44600	2·44564
$\bar{x}_2$	0·47363	0·47140
σ_1^2	0·32756	0·32745
σ_2^2	0·06347	0·06312

† See equations (7) and (8) for the definition of σ_l^2 and $\bar{x}_l$ ($l = 1, 2$).

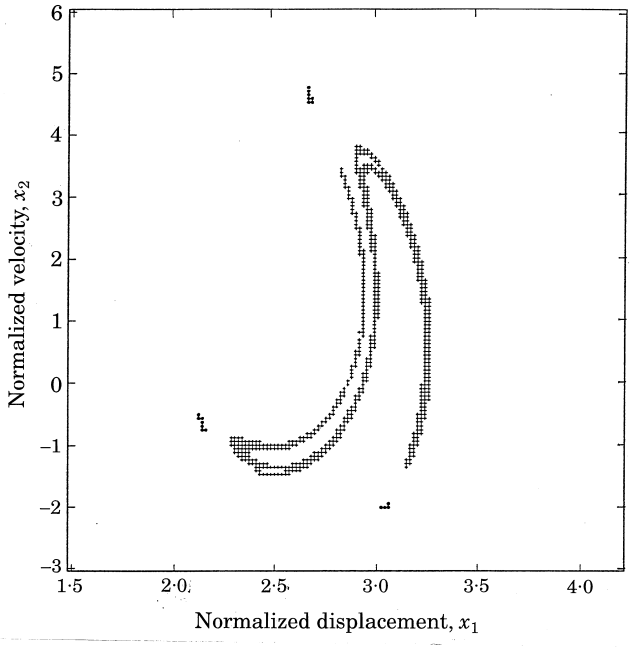

Figure 6. Persistent groups for the example system and for $\alpha_2 = 0{\cdot}02$. ●, Third order subharmonic attractor; +, strange attractor.

marked "2" in Figure 8 moves into the BOA for the strange attractor as can be seen in Figure 7(a) and some multiple domicile cells near the BOA for the sink cell (region marked "3" in Figure 7(a)) become part of the BOA for the third order subharmonic group (see Figure 8). Comparison of Figures 7(c) and 9 show how the BOA boundaries may become "blurred" when there is uncertainty in the system parameters. The blank cells in the region marked "1" in Figure 7(c) are part of the BOA for the third order subharmonic attractor when $\alpha_2 = 0{\cdot}02$ (see Figures 7(a)), but when α_2 is uniformly distributed over $0{\cdot}005 \leqslant \alpha_2 \leqslant 0{\cdot}035$ (i.e. Case 1) their probability of being absorbed in this attractor decreases and the probability of being absorbed in the strange attractor increases as shown in Figure 9. A similar trend is seen in the cells of the region marked "2" in Figures 7(c) and 9.

The computation times for the various steps in the implementation of CCMT on the example system are shown in Table 3 for a single α_2 value. The total CPU time to generate the data for both Figures 4 and 5 using equations (22)–(26) and the three α_2 values listed in Table 1 was about $3 \times (220 + 10) = 690$ s or 11·5 min on the Ohio Supercomputer Center CRAY Y/MP, with 96% of this time used for the generation of $\tilde{g}_{j,j'm}(\tau)$ (i.e., $3 \times 220 = 660$ s, or about 11·1 min). The same $\tilde{g}_{j,j',m}(\tau)$ were also used to generate the Figure 1–3 data. On the other hand, the total data generation time would have doubled if a Monte Carlo scheme were used to generate the data for Figures 4 and 5, since it would then be necessary to recompute the $g_{j,j'}(\tau)$ for each $P(\boldsymbol{\alpha})$ given by equations (36) and (37). Furthermore, this approach would not have yielded the information in Figures 1–3, which is important in order to understand the sensitivity of the structure of PG's to changes in the system parameters. It is also shown in Table 3 that the new algorithm used for the determination of the PG's, BOA's and their absorption probabilities (section 3.3) reduces the CPU time by a factor of about 20. The estimated reduction in storage requirements due to the new algorithms is by a factor of 2·5.

5. CONCLUSIONS

The CCMT proposed by Hsu [23, 24] is a powerful numerical technique for the global analysis of non-linear dynamical systems, and perhaps the only available feasible technique if the system equations do not satisfy the differentiability requirements of the analytical

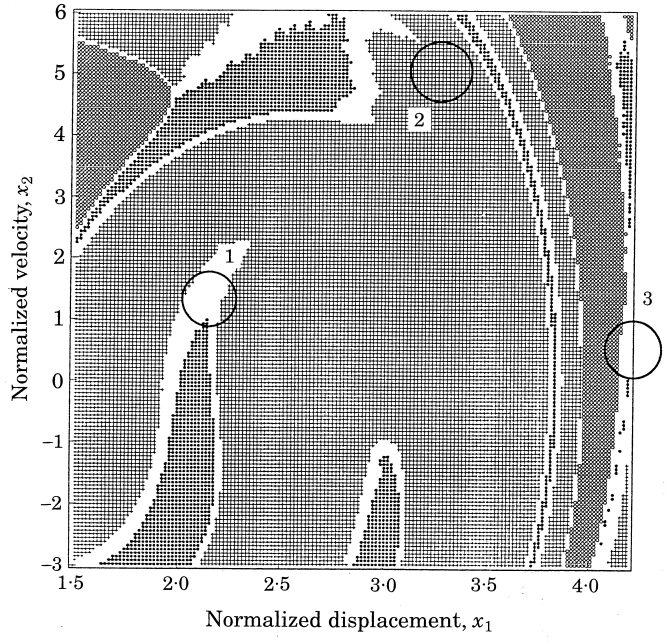

(a)

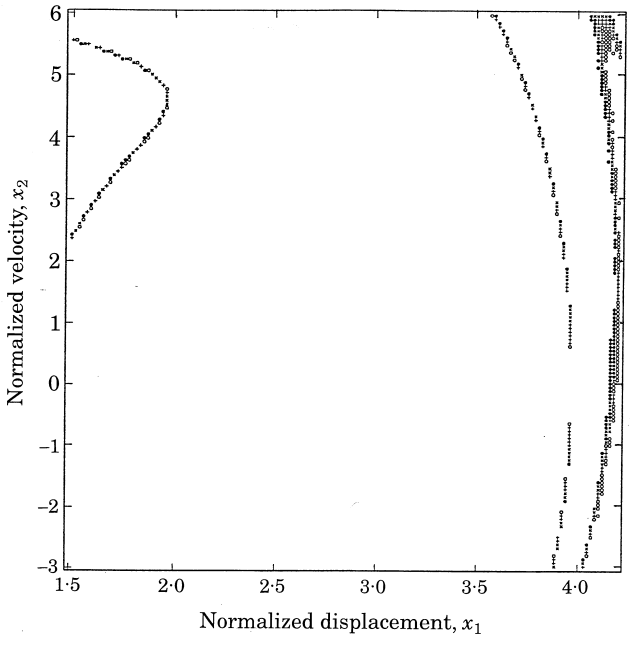

(b)

Fig. 7a and b

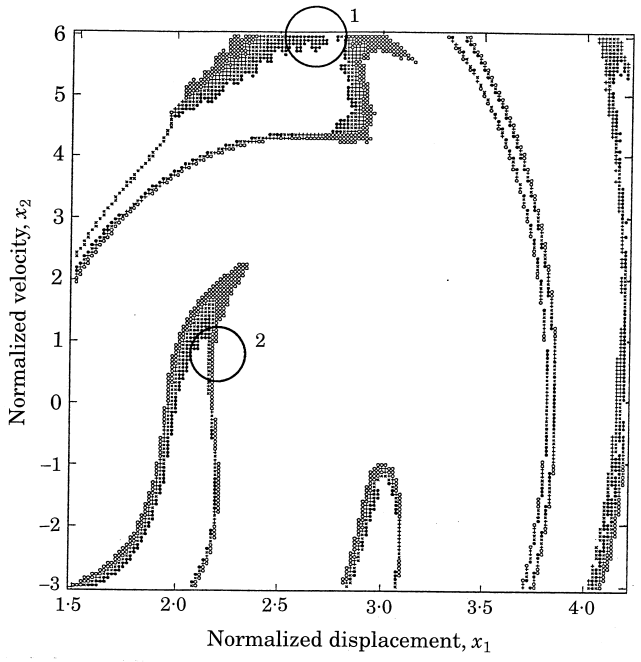

(c)

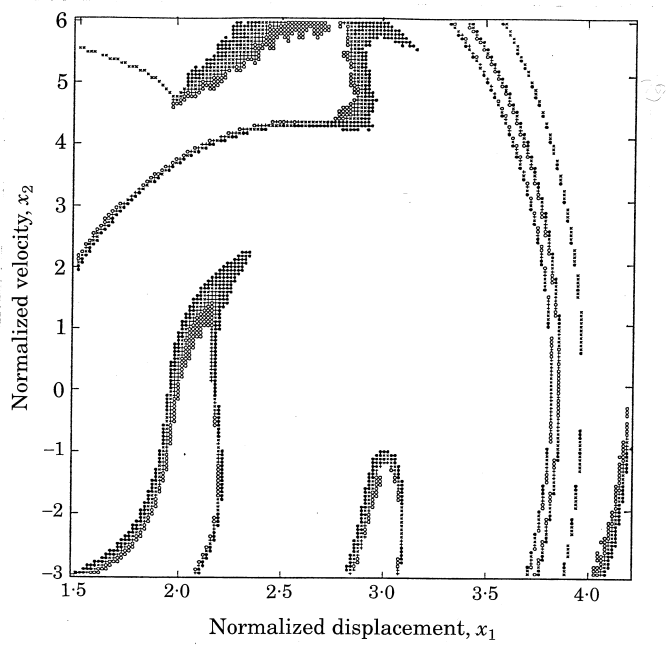

(d)

Figure 7. Basins of attraction (BOA's) of the example system for $\alpha_2 = 0{\cdot}02$ and absorption probabilities of the multple domicile cells. (a) BOA's for the sink cell (○), third subharmonic group (●), strange attractor (+) and multiple domicile cells (blank). (b) Absorption probabilities ($\rho^{\infty}_{1,i}$) of multiple domicile cells into the sink cell: ●, $0{\cdot}75 \leqslant \rho^{\infty}_{1,i} \leqslant 0{\cdot}99$; ×, $0{\cdot}50 \leqslant \rho^{\infty}_{1,i} \leqslant 0{\cdot}75$; +, $0{\cdot}25 \leqslant \rho^{\infty}_{1,i} \leqslant 0{\cdot}50$; ○, $0{\cdot}01 \leqslant \rho^{\infty}_{1,i} \leqslant 0{\cdot}25$). (c) Absorption probabilities ($\rho^{\infty}_{2,i}$) of multiple domicile cells into the third order subharmonic attractor: ●, $0{\cdot}75 \leqslant \rho^{\infty}_{2,i} \leqslant 0{\cdot}99$; ×, $0{\cdot}50 \leqslant \rho^{\infty}_{2,i} \leqslant 0{\cdot}75$; +, $0{\cdot}25 \leqslant \rho^{\infty}_{2,i} \leqslant 0{\cdot}50$; ○, $0{\cdot}01 \leqslant \rho^{\infty}_{2,i} \leqslant 0{\cdot}25$). (d) Absorption probabilties ($\rho^{\infty}_{3,i}$) of multiple domicile cells into the strange attractor: ●, $0{\cdot}75 \leqslant \rho^{\infty}_{3,i} \leqslant 0{\cdot}99$; ×, $0{\cdot}50 \leqslant \rho^{\infty}_{3,i} \leqslant 0{\cdot}75$; +, $0{\cdot}25 \leqslant \rho^{\infty}_{3,i} \leqslant 0{\cdot}50$; ○, $0{\cdot}01 \leqslant \rho^{\infty}_{3,i} \leqslant 0{\cdot}25$.

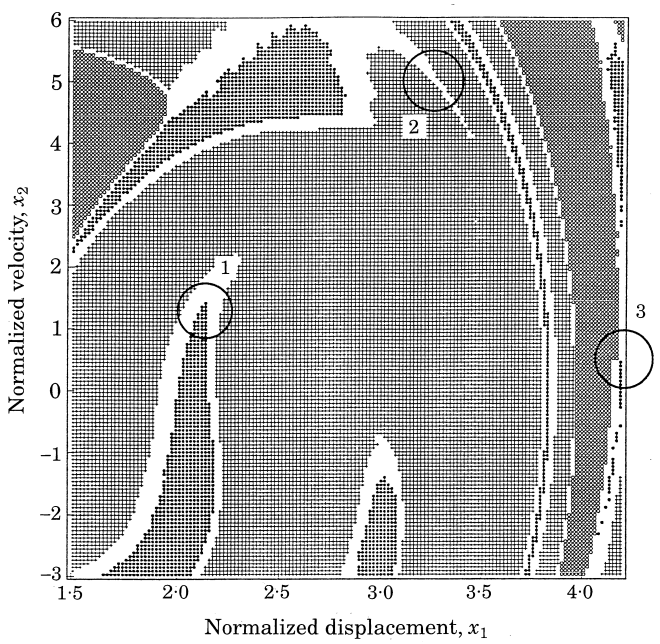

Figure 8. Basins of attraction (BOA's) of the example system for the sink cell (○), third subharmonic group (●), strange attractor (+) and multiple domicile cells (blank) for $\alpha_2 = 0{\cdot}01$.

techniques (see, e.g., reference [19]). Such a situation can be encountered, for example, in control systems with on/off controls. However, even with CCMT, computational requirements for global analysis can be still prohibitive for practical systems. This paper presents two algorithms based on a Chapman–Kolmogorov representation of system dynamics to reduce the computational requirements for CCMT. These algorithms are similar in spirit to the approach developed by Sun and Hsu [30] to reduce the computational time in the global analysis of non-linear random vibrations using CCMT, and are applicable in all situations in which the changes in the system parameters and dynamic variables are statistically independent. Section 4 illustrates that the new algorithms: (i) can speed up the determination of BOA's and BOA cell absorption probabilities in PG's by a factor of 20 and reduce the storage requirements by a factor of 2·5; and (ii) for systems with stochastic parameters, reduce the computational time needed to determine the probability distribution of PG's by a factor proportional to the number of PDF's that need to be considered if a unique PDF cannot be identified to represent the stochasticity in the system parameters.

TABLE 3

Comparison of computation times on a CRAY Y-MP for a single α_2 for the example system

Quantities determined	CCMT as described in section 2	New algorithms
$g_{j,j'}(\tau)$	220 s	220 s
Probability distribution of PG's from $\tilde{g}_{j,j',m}(\tau)$	10 s	10 s
PG's, BOA's and cell absorption probabilities into PG's	310 s	15 s

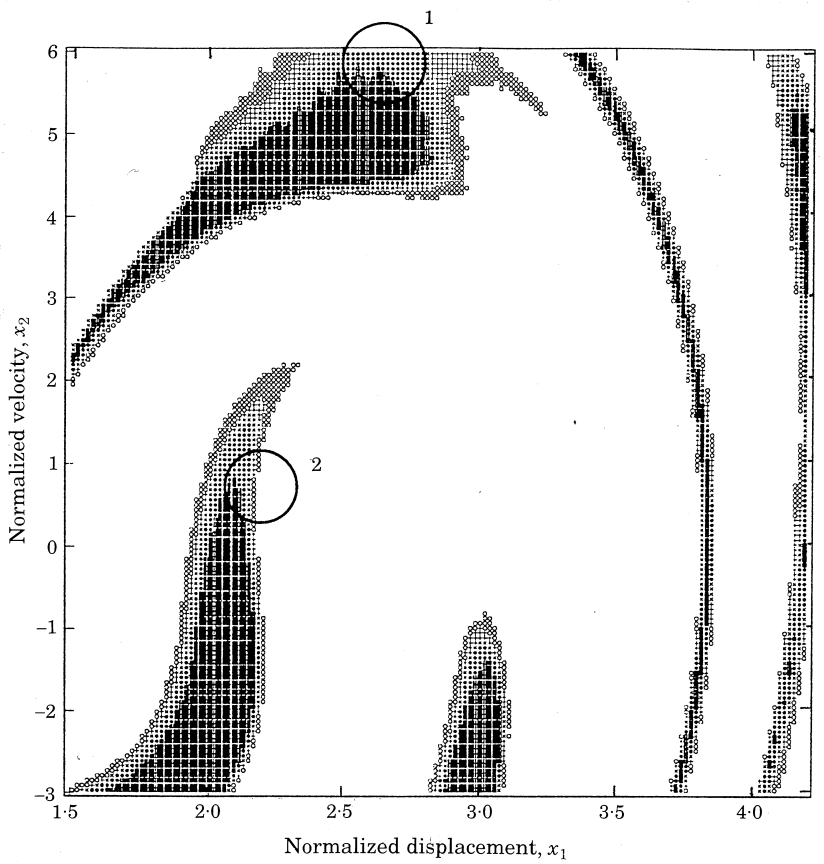

Figure 9. Absorption probabilities ($\rho^{\infty}_{2,i}$) of the multiple domicile cells into the third order subharmonic attractor for α_2 uniformly distributed (case 1): ■, $0{\cdot}99 \leqslant \rho^{\infty}_{3,i} \leqslant 1{\cdot}0$; ●, $0{\cdot}75 \leqslant \rho^{\infty}_{3,i} \leqslant 0{\cdot}99$; ×, $0{\cdot}50 \leqslant \rho^{\infty}_{1,i} \leqslant 0{\cdot}75$; $0{\cdot}25 \leqslant \rho^{\infty}_{1,i} \leqslant 0{\cdot}50$; ○, $0{\cdot}01 \leqslant \rho^{\infty}_{1,i} \leqslant 0{\cdot}25$.

Although CCMT has been mostly applied for the global analysis of mechanical systems so far, the authors believe that it is also a very useful technique in general for a comprehensive fault-tolerance/safety assessment of dynamical engineering systems with uncertainties on the parameters and/or initial conditions. Such uncertainties can arise from a variety of causes, including possible error on the experimentally determined quantities used in the design model, the possibility of component malfunction, human error and other stochastic parameter changes during operation (e.g., noise), as well as uncertainty on the monitored data. For these types of applications, the theoretical basis described in section 3.1 can be further extended to include systems in which the variations in dynamic variables and the system parameters are statistically dependent [38].

ACKNOWLEDGMENT

This study was partly supported by a grant from the Ohio Superconducting Center (PAS709-1).

REFERENCES

1. G. Cognet 1984 *Journal de Mechanique Theorique et Appliquee*, Numero special supplement, 7–44. Les etapes vers la turbulence dans l'ecoulement de Couette–Taylor entre cylindre coaxiaux.

2. S. Fauve 1984 *Journal of Mechanique Theorique et Appliquee*, Numero special supplement, 45–76. Transition vers la turbulence des ecoulement convectifs.
3. J. C. Roux, P. Richetti, A. Arneodo and F. Argoul 1984 *Journal de Mechanique Theorique et Appliquee*, Numero special supplement, 77–100. Chaos in a chemical system: towards a global interpretation.
4. P. Coullet and C. Tresser 1984 *Journal de Mechanique Theorique et Appliquee*, Numero special supplement, 217–240. Un scenario typique de la transition vers le chaos: la cascade de doublement de periode.
5. E. J. Kreuzer 1987 *International Series of Numerical Mathematics* **79**, 161–171. On the numerical study of bifurcation problems.
6. M. Hazewinkel 1985 *Bifurcation Analysis: Princples*, *Applications and Synthesis*, 13–30. Dordrecht: D. Reidel, Bifurcation phenomena—a short introductory tutorial with examples.
7. J. Awrejcewicz 1989 *Bifurcation and Chaos in Simple Dynamical Systems*. Singapore: World Scientific.
8. T. Kapitaniak 1991 *Chaotic Oscillations in Mechanical Systems*. Manchester: Manchester University Press.
9. R. H. Rand and D. Armbruster 1987 *Perturbation Methods*, *Bifurcation Theory and Computer Algebra*. New York: Springer-Verlag.
10. F. H. Busse and M. Sieber 1991 *International Series of Numerical Mathematics* **97,** 79–92. Regular and chaotic patterns of Rayleigh–Bernard convection.
11. F. K. Labisch 1991 *International Series of Numerical Mathematics* **97**, 243–248. Qualitative and quantitative behaviour of nonlinearly elastic rings under hydrostatic pressure.
12. C. H. Lamarque and J. M. Malasoma 1991 *International Series of Numerical Mathematics* **97**, 249–256. Computation of basins of attractions for three coexisting attractors.
13. F. Benedettini and G. Rega 1991 *International Series of Numerical Mathematics* **97**, 59–66. Periodic solutions leading to chaos in an oscillator with quadratic and cubic nonlinearities.
14. J. P. Eckmann and D. Ruelle 1985 *Reviews of Modern Physics* **57**, 617–656. Ergodic theory of chaos and strange attractors.
15. J. Q. Sun and C. S. Hsu 1991 *Journal of Sound and Vibration* **147**, 185–201. Effects of small random uncertainties on non-linear systems studied by the generalized cell mapping method.
16. M. Ding, C. Grebogi and E. Ott 1989 *Physical Review A* **39**, 2593–2598. Evolution of attractors in quasiperiodically forced systems: from quasiperiodic to strange nonchaotic to chaotic.
17. C. Froeschle 1984 *Journal de Mechanique Theorique et Appliquee*, Numero special supplement, 101–132. The Lyapunov characteristic exponents and applications.
18. D. Ruelle 1989 *Elements of Differentiable Dynamics and Bifurcation Theory*. San Diego: Academic Press.
19. S. Wiggings *Global Bifurcations and Chaos: Analytical Methods*. New York: Springer-Verlag.
20. C. S. Hsu and R. S. Guttalu 1980 *Journal of Applied Mechanics* **47**, 940–948. An unravelling algorith for global analysis of dynamical systems: an application of cell-to-cell mappings.
21. T. J. Garratt, G. Moore and A. Spence 1991 *International Series of Numerical Mathematics* **97**, 129–134. Two methods for the numerical detection of Hopf bifurcations.
22. D. Ruelle 1987 *Chaotic Evolution and Strange Attractors: The Statistical Analysis of Time Series for Deterministic Nonlinear Systems*. Cambridge: Cambridge University Press.
23. C. S. Hsu 1987 *Cell-to-cell Mapping: a Method for Global Analysis of Non-Linear Systems*. New York: Springer-Verlag.
24. C. S. Hsu 1980 *Journal of Applied Mechanics* **47**, 931–939. A theory of cell-to-cell mapping of dynamical systems.
25. V. K. Melkinov 1963 *Transactions Moscow Mathematics* **12**, 1–57. On the stability of the center for time periodic perturbations.
26. J. X. Xu, R. S. Guttalu and C. S. Hsu 1985 *International Journal of Non-linear Mechanics* **20**, 507–517. Domains of attraction for multiple limit cycles of coupled van der Pol equations by simple cell mapping.
27. C. S. Hsu and M. C. Kim 1986 *Journal of Statistical Physics* **38**, 735–761. Statistics of strange attractors by generalized cell mapping.
28. E. Ott 1981 *Review of Modern Physics* **53**, 665–671. Strange attractors and chaotic motions of dynamical systems.
29. H. M. Chiu and C. S. Hsu 1986 *Journal of Applied Mechanics* **53**, 702–710. A cell mapping method for non-linear deterministic and stochastic systems, part II: examples of application.

30. J. Q. Sun and C. S. Hsu 1990 *Journal of Applied Mechanics* **57**, 1018–1025. The generalized cell mapping method in nonlinear random vibration based upon short-time Gaussian approximation.
31. H. M. Taylor and S. Karlin 1984 *An Introduction to Stochastic Modeling*. Orlando, Florida: Academic Press.
32. C. S. Hsu and H. M. Chiu 1986 *Journal of Applied Mechanics* **53**, 695–702. A cell mapping method for non-linear deterministic and stochastic systems, part I: the method of analysis.
33. C. S. Hsu 1981 *Journal of Applied Mechanics* **48**, 634–642. A generalized theory of cell-to-cell mapping for nonlinear dynamical systems.
34. D. Bestle and E. Kreuser 1986 *Computer Methods in Applied Mechanics and Engineering* **59**, 1–9. A modification and extension of an algorithm for generalized cell mapping.
35. H. Stark and J. W. Woods 1986 *Probability*, *Random Processes and Estimation Theory for Engineers*. Englewood Cliffs, New Jersey: Prentice-Hall.
36. S. Yakowitz, J. E. Krimmel and F. Sziderovsky 1978 *SIAM Journal of Numerical Analysis* **15**, 1289–1300. Weighted Monte Carlo integration.
37. C. S. Hsu and H. M. Chiu 1987 *Journal of Sound and Vibration* **114**, 203–218. Global analysis of a system with multiple responses including a strange attractor.
38. T. Aldemir 1991 in *Probabilistic Safety Assessment and Management*, Vol. 2 (G. Apostolakis, editor), 1431–1436. New York: Elsevier. Utilization of the cell-to-cell mapping technique to construct Markov failure models for process control systems.